Reliability characterization and FEM modeling of power devices under repetitive power pulsing

F.Pozzobon, D.Paci, G. Pizzo, A.Buri, S. Morin, F.Carace, A.Andreini
STMicroelectronics
Cornaredo (MI), Italy
Fiorella.pozzobon@st.com

D. Gastaldi, E. Bertarelli, R. Lucchini, P. Vena
Politecnico di Milano
Milano, Italy
pasquale.vena@polimi.it

***Abstract*— In this work a combined experimental/numerical approach to describe the thermo-mechanical behavior of power devices under repetitive power pulsing is presented. Stress tests have been carried out on power DMOS implemented in Smart Power BCD technology with different Back-End Of Line (BEOL) schemes, including, for the first time, full Copper. Mechanical laboratory nano-indentation tests have been used to determine constituent properties of the metal layers. Thermo-mechanical 3D FEM modeling has been used to simulate a multi-cycle thermal loading of a whole power device with its package. Results from simulation have been qualitatively compared to experimental results.**

Keywords: Reliability; power devices; active cycling; thermo-mechanical fatigue

I. INTRODUCTION

Automotive products such as Anti-Lock Braking System (ABS) and Injector drivers are subjected to high energy pulses induced by re-circulation current of inductive loads. The pulse duration is typically in the range of 0.1-1msec for the above applications. The energy pulses generate high temperature gradients inside the power components: due to the device shrinkage the peak temperature may be above 300°C. Many phenomena that lead to the final device failure can be identified [1,2], namely: i) fatigue crack initiation within the elastic un-cracked oxide layers (high cyclic fatigue failure); ii) low cyclic fatigue failure due to alternating stress beyond the yield limit in the metal layers and ratcheting effects; iii) creep of the metal layers.

Thermo-mechanical stresses are induced by mismatch in Coefficient of Thermal Expansion (CTE) in the materials coupled to a cyclic change in temperature owed to the heating power input into the system. Both material properties and geometrical parameters of the device-packaging system strongly affect the thermo-mechanical stress state.

In general the understanding of the physics behind this failure mechanism is of utmost importance. Automotive field applications require strict mission profiles (in terms of number of pulses) and proper design guidelines are needed to not be "energy limited" as well as exploit potential for improved device on-resistance performances in advanced smart power technology platforms.

In this work for the first time repetitive power pulsing tests have been carried out on a power N-channel (ch.) laterally diffused MOS (LDMOS) with active clamp and two differing BEOL metal configurations: (1) mixed AlCu and thick top copper (2) full copper. Results from stress tests show an impressive advantage in the use of full copper back-end compared to a more traditional BEOL with AlCu, as presented in Section II.

In Section III the results of spherical nano-indentation tests [3,4] are presented with the aim of extracting materials constituent parameters for the metal layers in elastic and plastic regimes to be used in thermo-mechanical simulations.

The outcomes from experimental activity are qualitatively compared in Section IV to thermo-mechanical Finite Element simulations on the device-package system subjected to power cycling with the purpose to explain the different performance of the full Cu BEOL. A sequential coupling between thermal and mechanical analyses has been adopted for the 3D modeling of the whole device.

In Section V the experimental and simulated results are compared and discussed; in Section VI the conclusions are presented.

II. POWER PULSING TESTS

A power N-ch. LDMOS on 0.16um Bipolar CMOS DMOS (BCD) technology platform with active clamp has been submitted to repetitive power pulsing tests simulating the recirculation of an inductive load. The power component area was 0.76mm^2, 60V voltage class; an embedded NPN Bipolar Junction Transistor (BJT) connected as diode enables the temperature monitoring during the pulsing (see Figure 1 for the circuit schematic). The power N-ch. LDMOS has been designed with three thin metal levels plus a 4µm thick copper layer as top metal level. The first three thin metal layers are 0.3-0.5µm thick for both BEOL configurations with full copper being latest BEOL scheme for 0.11µm BCD technologies.

978-1-4799-0113-5/13/$31.00 ©2013 IEEE

Stress test is executed on samples assembled in Power SO plastic package, using an ARES-10 burn-in system (see Figure 2). Stress test boards are designed with a diagnostic circuit to detect failures (open/short) and a circuit to enable temperature measurement through the embedded NPN transistor. The energy value is not limited by passive components and is given by the current, the clamping voltage and the pulse length. The clamping voltage can be selected biasing an external pin.

Repetitive power pulsing test is carried out until the occurrence of an electrical short. The failure mechanism is correlated to thermo-mechanical stresses induced by mismatch in Coefficient of Thermal Expansion (CTE) in the materials coupled to a cyclic change in temperature owed to the heating power input into the system. Stress tests have been carried out at relatively low current density levels, therefore electro-migration phenomena are not responsible for the device failure (see Figure 3: simulation by R3D tool from Silicon Frontline [6] of current density on top n-metal, and n-1 metal). Failure occurs because of inter-metal oxide cracking, due to metal plastic deformation (see Figure 4), leading to metal short when the metal extrudes inside the crack (see Figure 5 for AlCu thin metal) [5, 6, 7].

The failure statistic can be described by the Weibull distributions. Figure 6 depicts the Weibull distributions from stress tests on mixed AlCu with thick Copper top metal versus full Copper samples.

1ms pulses with 20% duty cycle were applied to power devices at 200°C above the junction temperature reproducing aggressive automotive mission profiles. As a result the lifetime of the full Cu BEOL is improved by a factor ~10-100 respect to the mixed AlCu and Cu BEOL. The improvement comes primary from the replacement of AlCu thin metal layers with Cu thin metal ones, the top metal being exactly the same for both BEOL schemes. The Failure analysis carried out on several devices did not highlight thin metal deformation similar of AlCu in case of full Cu BEOL (see Figure 7).

The boost in lifetime for full Copper BEOL has been confirmed using a 10um thick Copper top metal. It is also observed that the 10um thick Copper acts more effectively as a heat sink, therefore the transistor is on average a little bit colder at same energy.

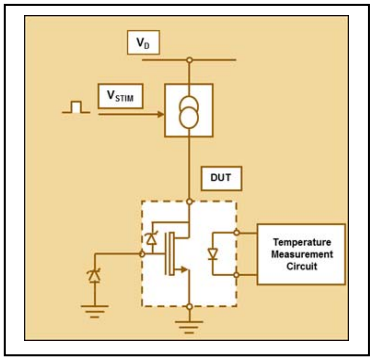

Figure 1. Simplified circuit diagram

Figure 2: OLT test system

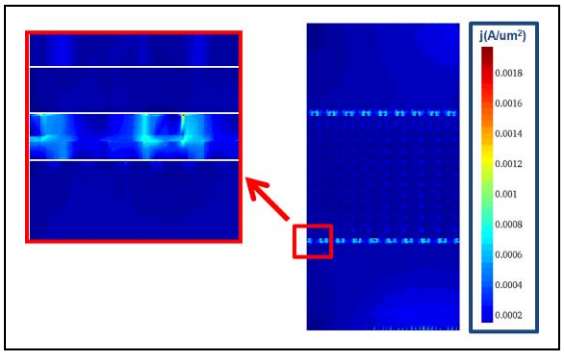

Figure 3. R3D (Silicon Frontline) current density simulation at metal n-1 during a representative stress test at Vds=62.5V, Ids=1A, Tj=175°C. AlCu thin metal, thick Copper top metal

Figure 4. n-1 metal deformation due to thermo-mechanical stress. AlCu thin metal lines

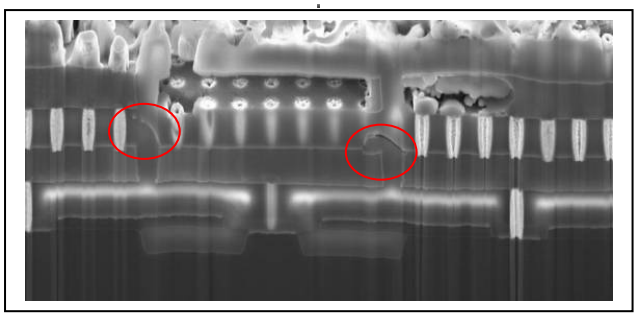

Figure 5: short between metal due to metal extrusion inside oxide crack. AlCu thin metal lines

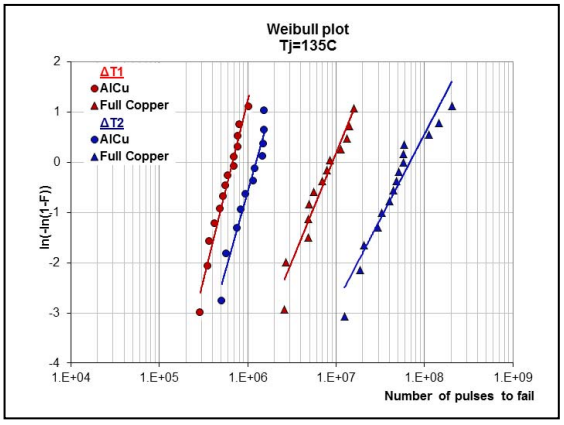

Figure 6. Weibull distributions from repetitive power pulsing. Tests have been carried out pulsing at ΔT1>ΔT2 in the range of 200°C above the junction temperature Tj=135°C.

Figure 7: Damascene Cu thin metal lines on a device submitted to several million power cycles.

III. METAL LAYERS CHARACTERISATION:NANO-INDENTATION TESTS

Spherical indentation tests allow extracting the yield stress-plastic strain relationship for hardening materials without making ideal tensile or compressive tests. [3].

The indentation modulus, related to the elastic behavior of the metal coating, was determined by applying the Field and Swain theory. All samples have been placed on measurement position within a temperature-controlled cabinet. The ambient temperature was set to 28°C and kept constant throughout each experiment.

Figure 8 shows the yield-stress (flow stress) versus representative plastic strain for the Aluminum and Copper layers from the nano-indentation experiments. Average indentation modulus is 80 GPa and 120 GPa for Aluminum and Copper coatings, respectively. Assuming a Poisson ratio υ=0.34, the resulting Young moduli are 76 GPa and 118 GPa for Aluminum and Copper layers, respectively. The Copper coatings exhibited a yield stress higher than that found for the Aluminum layers over the whole range of plastic strain investigated; in particular, at 4% plastic strain, a yield stress of about 180 MPa and 300 MPa is found for Aluminum and Copper, respectively.

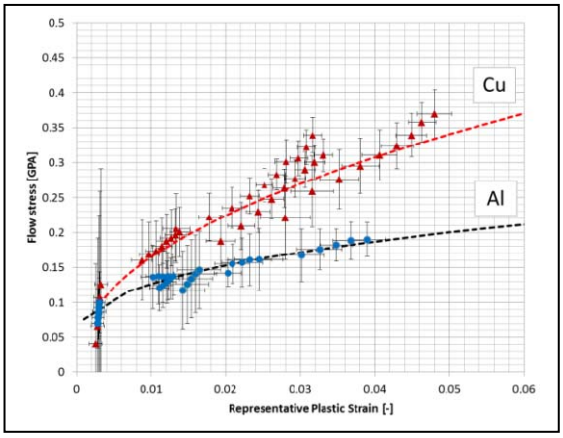

Figure 8: Yield stress - plastic strain relationship for Aluminum and Copper coatings (vertical and horizontal bars indicates standard deviations).

I. FINITE ELEMENT MODEL FOR THE POWER DEVICE

Same device used for the pulsing tests has been modeled to enable a qualitative comparison between experimental results and FEM simulation outcomes.

A. Thermal analysis

Only half of the device has been modeled assuming a symmetry plane. Figure 9 shows the geometric model of the device with mold compound and silicon surround. In the geometrical model the polymeric mold on the top of the device is 100 μm thick and is 600 μm wide (all around the device).

The geometrical model includes the temperature sensor. The real device is composed by a stacking of several thin layers which are characterized by a complex structure. The top metal level has the same layout as in the real device, whereas for the top interconnecting vias arrays a re-grouping approach has been adopted. For all the other layers (thin conductors and inter-metal dielectrics) a layer-by-layer homogenization is adopted; namely, each device layer is composed by a homogeneous equivalent material, herein referred generally as "metal" or “IMD”. The thin metal layers exhibit a spatial pattern made of alternate Source and Drain fingers, where the amount of the non-metal component is less than 10% of the total volume; therefore, it can be expected that a homogenized model would properly represent the mechanical behaviour of such layers at the length scale of the device.

As condition at the boundary, on the symmetry plane the adiabatic condition has been applied.

Total heat power input into the system was prescribed as a volumetric heat source applied on the "heater layer" (i.e. the active Silicon surface portion of the DMOS component, which is dissipating the applied power). Five thermal cycles (5x5 ms) were simulated by prescribing a heat power input for 1 ms having magnitude consistent with the experimental data.

The volumetric heat source Q during a single thermal cycle was simulated according to the following temporal description:

$$Q = \overline{Q} \quad \text{for} \quad 0 < t < 1\text{ms}$$

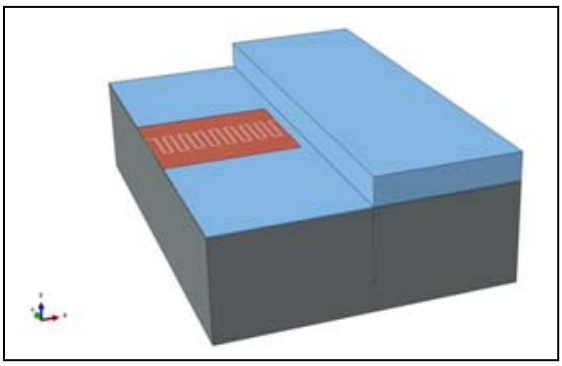

Figure 9. Geometric model: red sub-domain is the device (top metal layout), blue regions represent the surrounding mold (on top side, a portion is removed to show the device) and the silicon substrate (on bottom side)

$$Q = 0 \quad \text{for} \quad 1\text{ms} < t < 5\text{ms} \tag{1}$$

$\overline{Q}$ was calculated according to the following relationship:

$$\overline{Q}(units) = \frac{q(units)}{t_{hl}} \tag{2}$$

where t_{hl} is the thickness of the "heater layer": a fictitious layer - the thermal properties of which were assumed to be those of the silicon material – with a thickness of 300 nm. q is the heat source input per unit area (equal to 74.7 W/mm^2) The size of the "heater layer" is equal to the size of the DMOS component.

In the three-dimensional domain of the "heater layer" the following field equations were solved:

$$\nabla \bullet (k \nabla T) - c \frac{\partial T}{\partial t} = \overline{Q}; \tag{3}$$

the field equation to be solved in the rest of the model was:

$$\nabla \bullet (k \nabla T) - c \frac{\partial T}{\partial t} = 0 \tag{4}$$

The material parameters assigned to each material of the device layers and of the package are the thermal conductivity (k) and the heat capacity (c). A temperature-dependent thermal conductivity of silicon has been assumed.

The Finite Element analyses were run by using the commercial code ABAQUS (version 6.10) [9]. In Figure 10 is reported the simulated temperature map during a stress test.

B. Thermo-mechanical analysis

Thermo-mechanical analyses were carried out by means of sequential weakly coupled equations of the thermo-mechanical problem. The assumption at the basis of the weakly coupled approach implies that the temperature field will affect the stress distribution through the heterogeneous distribution of the coefficient of thermal expansion of the materials, while stress within the material does not affect the temperature distribution.

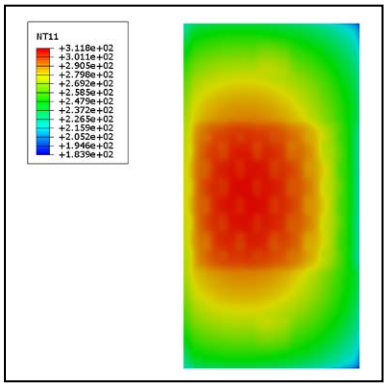

Figure 10. Example of temperature field at stress test condition

The temperature variation with respect to a reference temperature value will generate a dilatation of the device materials, of the molding polymer and of the silicon substrate, which is proportional to the coefficient of thermal expansion and to the temperature variation. The heterogeneous distribution of the coefficient of thermal expansion induces a mismatch of thermal strains between adjacent materials; the geometric compatibility between bonded materials (different layers of the device and the bonding between the device and the molding) constrains the free expansion of each component thus inducing a state of stress.

The mechanical behavior of the material is described through constitutive equations governing the stress-strain relationships. The silicon substrate and the mold are described by using linear equations representing a linear elastic isotropic material response. The Copper and Aluminum have been modeled as isotropic elastic-plastic materials. The development of plastic strains follows the Von Mises plasticity flow theory with a combined isotropic/ kinematic work hardening rule.

Isotropic work hardening material model assumes that when the state of stress reaches the elastic limit, plastic strains develop and the elastic domain expands isotropically. The kinematic hardening rule assumes that the yield surface translates, without rotation in the stress space. In a combined isotropic/kinematic hardening model both extension and translation of the elastic limit surface occur. Both kinematic and combined hardening models can account for the Boushinger effect [8] which is characterized by a progressive plastic strain accumulation upon a cyclic applied stress.

The evolution law of the combined hardening rule consists of two components: a non-linear kinematic hardening, which accounts for the translation of the limit surface in the principal stress space by introducing the "back stress" α_{ij} and the isotropic hardening component, which accounts for the change of size of the limit surface. This latter is achieved by changing the equivalent stress σ^0 as a function of an equivalent plastic strain (scalar function of the plastic strain tensor).

In such a formulation, the limit surface for a Von Mises type material is given by

$$\phi = \sqrt{\frac{3}{2}\left(S_{ij} - \alpha_{ij}\right)\left(S_{ij} - \alpha_{ij}\right)} - \sigma^0\left(\overline{\varepsilon^{pl}}\right) < 0 \qquad (5)$$

Sij is the ij component of the deviatoric stress tensor and $\sigma^0\left(\overline{\varepsilon^{pl}}\right)$ is the yield stress of the work hardening material, a function of a scalar measure of the total equivalent plastic strain $\overline{\varepsilon^{pl}}$ at each time instant. The equivalent plastic strain is defined as:

$$\overline{\varepsilon^{pl}} = \sqrt{\frac{2}{3}\varepsilon_{ij}^{pl}\varepsilon_{ij}^{pl}} \qquad (6)$$

In definition (6) the summation over repeated index is assumed.

In general the yield stress can also be a function of temperature and of strain rate. In the present work, yield stress is assumed as a function of the plastic strain only.

The components of the stress tensor are calculated at each time instant according to the following relationship:

$$S_{ij} = \frac{E}{1+\nu}\left(\varepsilon_{ij}^{e} - \frac{1}{3}\delta_{ij}\varepsilon_{kk}^{e}\right) \qquad (7)$$

where δ_{ij} is the Kronecker symbol; the Young Modulus (E) and the Poisson ratio (υ) to be used in (7) have been obtained from nano-indentation test on Aluminum and Copper. In (7) ε^{e}_{ij} are elastic strain components which are related to the total strain ε_{ij} according to the additive relationship

$$\varepsilon_{ij} = \varepsilon_{ij}^{e} + \varepsilon_{ij}^{pl} + \alpha\Delta T\delta_{ij} \qquad (8)$$

Last term in (8) represents the thermal strain proportional to the coefficient of thermal expansion and to the temperature increment with respect to a reference (initial) temperature.

The function of evolution of yield stress with the plastic strain $\sigma^0\left(\overline{\varepsilon^{pl}}\right)$ used in (5) was modeled in the following form:

$$\sigma^0\left(\overline{\varepsilon^{pl}}\right) = \sigma_0 + A\left(\varepsilon^{pl}\right)^n \qquad (9)$$

From the relationship between yield stress and equivalent plastic strain reported in Figure 8, the following values are obtained: σ_0=50MPa for both Aluminum and Copper, A=500MPa for Aluminum and 1330MPa for Copper, n=0.4 for Aluminum and n=0.5 for Copper. The other materials in the device have been modeled as isotropic linear elastic.

C. Results

Figure 11 shows the uniaxial response to cyclic stress loading with asymmetric stress reversal (maximum tensile stress 200 MPa, maximum compressive stress 100 MPa). In this way, a comparison between an isotropic and a combined isotropic/kinematic hardening model is provided. In figure 11, the stress-strain response to uniaxial cyclic loading with prescribed stress is reported in a three cycle example. The stress strain response with isotropic hardening is characterized by a superposition of the stress-strain response over the cycles; whereas, a progressive increase of strain is observed with cycles for the combined model. Therefore a progressive accumulation of plastic strain is found for the combined model; whereas, a steady stress-strain cycle is found with the isotropic hardening rule.

Figure 12 shows the time evolution of the equivalent plastic strain in a representative integration point within a. the Copper layer, b. the Aluminum layer. Isotropic hardening simulations have shown that an increase of plastic strain occurs in the Copper/Aluminum layers with a maximum equivalent plastic strain of 0.5%/2% in case of Copper and Aluminum respectively; whereas, a steady increase of plastic strain (up to 1.9% for Copper and up to 4% for Aluminum) has been found on the five cycles simulation in case of combined hardening. This clearly indicates that kinematic or combined hardening of the metal material may have a relevant effect on the lifetime predictions of the devices.

The thermo-mechanical analysis put in evidence that the most critical layer is the Metal 3 (i.e. the thin metal level just below the thick top metal layer), in which the highest values of the plastic strain and of the Von Mises stress were found. Figure 13 shows a comparison between the von Mises stresses distributions in the Aluminum metal 3 layer at the end of the first cycle and at the end of fifth cycle.

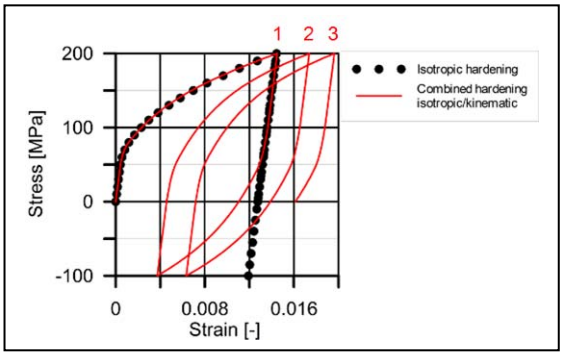

Figure 11: Stress-strain response to uniaxial cyclic loading with prescribed stress; comparison between isotropic hardening and combined isotropic/kinematic hardening (3 distinct cycles in red for the combined hardening; note in case of isotropic hardening the superposition of the stress-strain response, dotted curve).

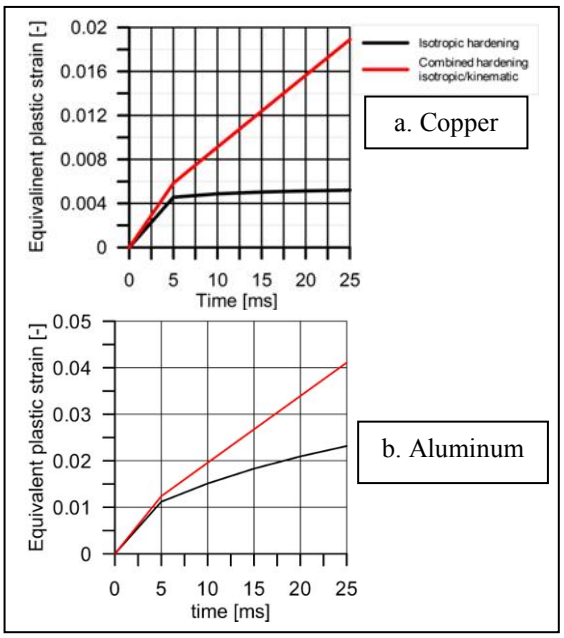

Figure 12: Effect of the hardening model: equivalent plastic strain in a.Copper, b. Aluminum at the end of each load cycle (five cycles have been simulated).

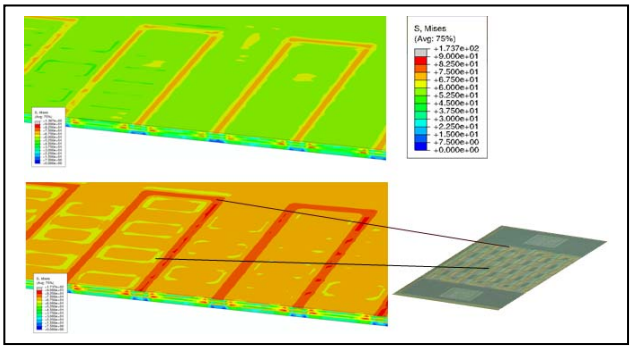

Figure 13. Von Mises stress distribution for the Aluminum metal 3 layer at the end of the first cycle (top) and at the end of the fifth cycle (bottom). The stress is higher in the IMD between top metal fingers. Optical image is related to an unstressed device at metal 3 level.

The contour map shows that, at the end of the fifth cycle, a slightly higher Von Mises stress is found, with respect to the first cycle. In particular, an increase of Von Mises stress from 70MPa to 80MPa (approximate values) has been found.

Figure 14 shows the contour maps of the equivalent plastic strain at the end of first cycle and at the end of the fifth cycle. The maps show a significant increment of plastic strain upon cycle loading: the equivalent plastic strain increases from 1% (end of first cycle) to 4% (end of fifth cycle). For comparison purposes, an image of the same layer, after removal of the thick top metal level, of a device subject to the energy pulsing experiment is reported on Figure 15. The grazing light image shows a smeared damage on the Aluminum layer following a pattern similar to that found on the plastic strain contour of the finite element model.

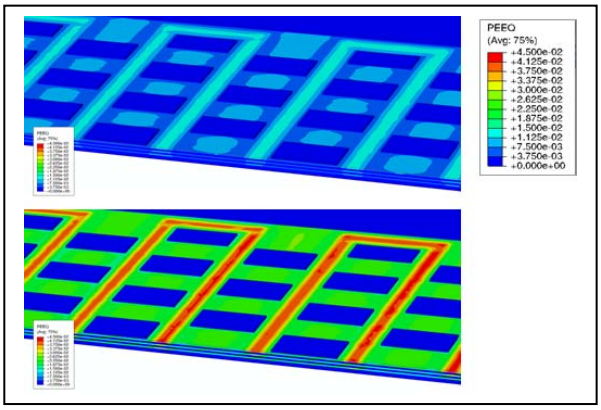

Figure 14. Equivalent plastic strain distribution for the Aluminum metal 3 layer at the end of the first cycle and at the end of the fifth cycle. The strain is higher in the IMD between top metal fingers. Blue squares are re-grouped vias3

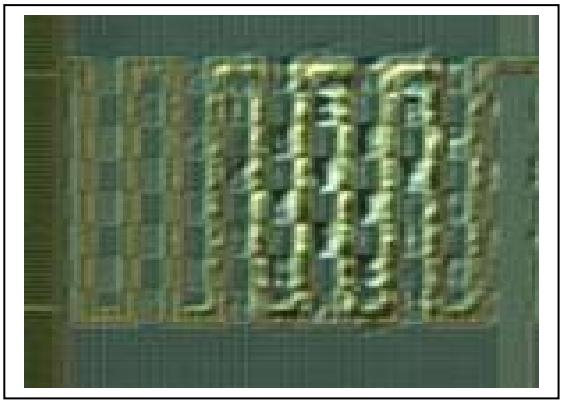

Figure 15. Optical Image (grazing light) at Aluminum metal 3 layer of a sample submitted to repetitive power pulses: AlCu and thick Copper mixed BEOL

The finite element analysis has been carried out also in the case of a full Copper BEOL, by replacing the AlCu equivalent thin metal layers with Copper layers. As shown in 16 in comparison with the Copper/Aluminum device, the Von Mises stress within the metal 3 layer does not change appreciably (about 80MPa for both full Copper and Aluminum/Copper BEOL).

Also, a lower equivalent plastic strain has been found in the metal 3 layer for the full Copper device in the order of 3% (see Figure 17 and Figure 18 as qualitative comparison with experimental evidence) whereas an equivalent plastic strain about 30% higher was found for the Aluminum/Copper BEOL.

II. DISCUSSION

The finite element simulations allowed achieving the following results: identification of critical locations within the device where damage can be expected to develop over repetitive cyclic pulsing; determination of inelastic strain accumulation over thermal cycles.

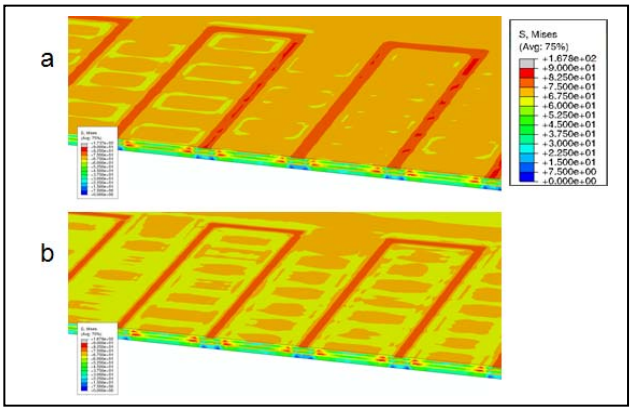

Figure 16. Von Mises stress distribution at the end of the fifth cycle for the aluminum/copper BEOL (a) and for the full Copper BEOL (b)

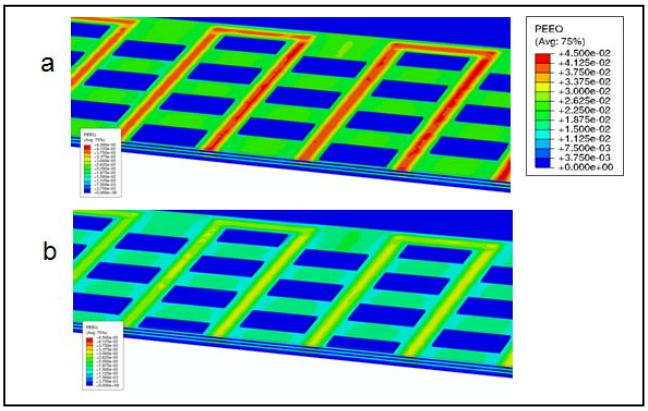

Figure 17: Equivalent plastic strain distribution at the end of the fifth cycle for the Aluminum/Copper BEOL (a) and for the full Copper BEOL (b)

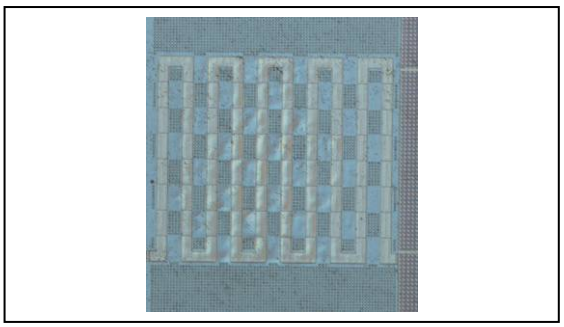

Figure 18: Optical Image (grazing light) at Copper metal 3 layer of a sample submitted to repetitive power pulses: full Copper BEOL

Thermo-mechanical finite element simulations have shown that plastic strains increases upon cycle loading and that the amount of strain increase per cycle is strongly dependent on the assumption on kinematic hardening of the metal layers.

The results of the numerical simulations have clearly shown that the device has specific locations with concentration of permanent (plastic) strain and peaks of tensile stress components; it can be speculated that these are locations of potential material failure limiting the life of the device: the thin n-1 metal level is more solicited in the region between source and drain fingers of thick top metal level, as confirmed by physical analysis outcomes.

Finally, the analysis of thermo-mechanical simulation of full Copper BEOL indicates that a full Copper device, being characterized by lower plastic strain with respect to an Aluminum/Copper device, would be affected by a reduced ratcheting effect (accumulation of plastic strain), as well.

This finding qualitatively explains the better performance of Copper seen during repetitive power pulses tests.

Since the increasing stress in the inter-metal oxide layers is due to the accumulation of plastic deformation within the thin metal lines, Copper conductor boosts the device lifetime, owed to its greater strenght, as experimentally verified through the end-of-life repetitive power pulsing tests presented in Section II.

The improvement in the mechanical performance of Copper is verified by the layer characterisation through nano-indentation tests.

III. CONCLUSIONS

In this work experimental results from repetitive power pulsing tests have been reported, showing for the first time a boost in the lifetime of Copper BEOL compared to mixed Aluminum/Copper BEOL.

The mechanical behavior of metal layers has been characterized through nano-indentation laboratory tests with the purpose to probe mechanical properties of materials at the real length scale of device. The laboratory tests allowed obtaining the values of the constitutive parameters to be used in the finite element model adopted for thermo-mechanical simulations which have been capable to qualitatively explain the experimental evidence.

Furthermore, the developed simulation setup, in which part of the layout features have been explicitly modeled and partly simplified adopting homogenized properties, has shown its effectiveness in identifying critical regions in the power component and can be a useful tool to support the device design. The numerical modeling of the failure scenarios can be further improved by developing a two scales approach in which a detailed description of the geometric patterns is included. The model at the device scale will provide the boundary conditions for the local scale models, where geometric features of those metal layers that have been homogenized in the present model are fully described. This approach is being adopted to enable a finer analysis of critical design parameters to further increase the device performances especially in case of AlCu BEOL.

The results obtained in this work highlight how a full Copper BEOL, now utilized in the newest BCD technology

platforms at 0.11µm, can give additional advantages, relevant to the Smart Power application requirements, compared to those already known in CMOS technologies, like the increased electro-migration performances vs. Aluminum material.

REFERENCES

[1] Shaw M.C., "High-Performance Packaging of Power Electronics," MRS Bulletin, Vol. 28 (2003), pp. 41-50.

[2] Smorodin T., Bohm C., Gaspar J., Schmidt M., Paul O., Stecher M., "Modeling and improvement of a metallization system subjected to fast temperature cycle stress," Proc of EuroSimE 2008, Freiburg im Breisgau, Germany, pp. 1-6.

[3] Taljat B., Zacharia T., "New analytical procedure to determine stress-strain curve from spherical indentation data," Int J Solids Struct, Vol. 35 (1998), pp. 4411–4426.

[4] Smorodin T,Wilde J., Alpern P.,Stecher M.,"A Temperature-Gradient-Induced Failure Mechanism in Metallization Under Fast thermal Cycling", IEEE Transactions on Dev. and Mat. Rel. 2008,Vol 8, n.3 pp 590-599.

[5] Smorodin T,Wilde J., Alpern P.,Stecher M.,"Investigation and Improvement of fast temperature cycle Reliability for DMOS-related conductor path design", IRPS 2007 pp 486-491.

[6] Silicon Frontline Technology, 595 Millich Dr., suite 206. Campbell, CA 95008, USA www.siliconfrontline.com. R3D is a resistive 3D extraction and analysis product for large resistive structures like power devices.

[7] Computational Inelasticity, J.Simo and T.J.R Hughes, Interdisciplinary Applied Matematics, volume 7, ISBN 0-387-97520-9, Springer Verlag New York Berlin Heidelberg, 1998

[8] Abaqus Theory Manual (Version 6.10). Providence, RI: DS SIMULIA; 2010.